The Acacia Gum Arabinogalactan Fraction Is a Thin Oblate Ellipsoid: A New Model Based on Small-Angle Neutron Scattering and Ab Initio Calculation

C. Sanchez,* C. Schmitt,† E. Kolodziejczyk,† A. Lapp,‡ C. Gaillard,§ and D. Renard§

*Laboratoire de Science et Génie Alimentaires, ENSAIA-INPL, F-54505 Vandoeuvre-lès-Nancy cedex 5, France; †Department of Food Science, Nestlé Research Center, CH-1000 Lausanne 26, Switzerland; ‡Laboratoire Louis Brillouin, CEA Saclay, 91191 Gif-sur-Yvette cedex, France; and §Unité de Recherches sur les Biopolymères, Interactions, Assemblages, INRA Centre de Nantes BP 71627, 44316 Nantes cedex 3, France

ABSTRACT Acacia gum is a branched complex polysaccharide whose main chain consists of 1,3-linked β-D-galactopyranosyl units. Acacia gum is defined as a heteropolysaccharide since it contains ~2% of a polypeptide. The major molecular fraction (F1) accounting for ~88% of the total acacia gum mass is an arabinogalactan peptide with a weight-average molecular weight of 2.86×10^5 g/mol. The molecular structure of F1 is actually unknown. From small angle neutron scattering experiments in charge screening conditions, F1 appeared to be a dispersion of two-dimensional structures with a radius of gyration of ~6.5 nm and an inner dense branched structure. Inverse Fourier transform of F1 scattering form factor revealed a disk-like morphology with a diameter of ~20 nm and a thickness below 2 nm. Ab initio calculations on the pair distance distribution function produced a porous oblate ellipsoid particle with a central intricated "network". Both transmission electron microscopy and atomic force microscopy confirm the thin disk model and structural dimensions. The model proposed is a breakthrough in the field of arabinogalactan-protein-type macromolecules. In particular, concerning the site of biosynthesis of these macromolecules, the structural dimensions found in this study would be in agreement with a phloem-mediated long-distance transport. In addition, the structure of F1 could also explain the low viscosity of acacia gum solutions, and its ability to self-assemble and to interact with proteins.

INTRODUCTION

Arabinogalactan-protein/peptide (AGP, AG-peptide) type biological macromolecules are widely distributed in the plant kingdom, probably occurring in every cell of every plant from bryophytes to angiosperms (1). They are thought to have various functions in plant growth and development, including signaling, embryogenesis, and programmed cell death (1–3). Certain AGPs, particularly those found in plant exudate gums, are also of commercial interest for the valuable chemical properties that they confer in various industrial applications (3). AGPs can be located in the cell wall, on the outer side of the plasmalemma, in vacuoles, in intercellular spaces, and in different secretions and mucilage (4). AGPs containing exudate gums are produced by many trees and shrubs as a natural defense mechanism, particularly in semi-arid regions. When the plant's bark is injured, an aqueous gum solution is exuded to seal the wound, preventing infection and dehydration of the plant. The solution dries on contact with air and sunlight to form hard, glass-like lumps that can be easily collected (5). Acacia gum, or gum arabic, is the oldest and best known of all natural gums. Its use can be traced back to the third millennium BC, the time of the ancient Egyptians. Although acacia gum has also been used as an adhesive in modern times, the most important applications are in the food, pharmaceutical, cosmetic, and lithography industries (1).

Acacia gum is a branched, neutral or slightly acidic, complex polysaccharide obtained as a mixed calcium, magnesium, and potassium salt. The main chain consists of 1,3-linked β-D-galactopyranosyl units with 1,6-linked β-D-galactopyranosyl side chains that in turn carry large amounts of α-arabinosyl residues and lesser amounts of β-glucuronosyl and other residues. Both the main and the side chains contain units of α-L-arabinofuranosyl, α-L-rhamnopyranosyl, β-D-glucuronopyranosyl, and 4-O-methyl-β-D-glucuronopyranosyl, the last two mostly as end units (6). Acacia gum is composed of 64 ramified 1,3-linked homogalactan symmetrically arranged subunits, each of molecular mass 8000 g/mol (7).

Acacia gum is defined as a heteropolysaccharide since it contains ~2% of a polypeptide (8). Acacia gum is also described as heteropolymolecular because it has, on the one hand, a variation in monomer composition and/or in the linking and branching of the monomer units and, on the other hand, a molecular mass distribution. The consequence of this heterogeneity was reflected through the molecular species collected after fractionation of acacia gum and the mode of both separation and detection used. In general, three main fractions can be isolated by hydrophobic interaction chromatography (9). Analysis of the fractions showed that each contained similar proportions of the various sugars and differed essentially in their molecular masses and protein contents. The bulk of the gum (88.4 wt % of the total) was shown to comprise an AG-peptide fraction with a weight-average molecular weight ($\bar{M}_w$) of 2.86×10^5 g/mol and a low protein content (0.35 wt %). This fraction will be called

Submitted March 19, 2007, and accepted for publication May 21, 2007.

Address reprint requests to C. Sanchez, Tel.: 33-3-83-59-57-88; Fax: 33-3-83-59-58-04; E-mail: Christian.Sanchez@ensaia.inpl-nancy.fr.

Editor: Jill Trewhella.

0006-3495/08/01/629/11 $2.00

doi: 10.1529/biophysj.107.109124

AG and F1 (Fraction 1) in the following to match most of the literature. The second major fraction (10.4 wt % of the total) was identified as an AGP with a molecular weight of 1.86×10^6 g/mol and contained a greater proportion of protein (11.8 wt %). The third minor fraction (1.2 wt %) will consist of one, or possibly two, glycoproteins (GPs). One of the GPs had a molecular weight of 2.5×10^5 g/mol and the highest protein content (47.3 wt %). The proteinaceous component of the first two fractions had similar amino acid distributions, with hydroxyproline and serine being the most abundant. The amino acid composition of the third fraction was significantly different, with aspartic acid being the most abundant.

The tertiary structure of the fraction with species of largest molecular weight, AGP, has been described in terms of a ''wattle blossom'' macromolecular assembly by virtue of which few (~5) discrete polysaccharide domains of $\bar{M}_w \sim 2.10^5$ g/mol are held together by a short peptide backbone chain (10). The key experimental evidence to support this hypothesis showed that hydrolysis of the AGP fraction with a protease produced a fivefold reduction in molecular weight and that these fractions were no longer prone to proteolysis. The shape of this macromolecule would be a kind of spheroidal random coil. An alternative model was proposed, describing the acacia gum GP as a statistical model with a fundamental 7000 g/mol subunit, where polysaccharide side chains attach to a polypeptide backbone of probably more than 400 residues (~150 nm long; 5 nm diameter; axial ratio ~30:1) in a highly regular and ordered fashion (every 10–12 residues repetitive peptide units), forming a ''twisted hairy rope'' (11). This model would be consistent with the fact that large macromolecules, like AGPs, migrate by reptation through a primary cell wall with a porosity of 4–5 nm (12).

The tertiary structure of the main molecular fraction of acacia gum, AG, has never before been studied. This fraction has been identified so far as the main fraction and would consequently play a key role in the functional properties of the whole gum. Previous work performed in the laboratory aimed to characterize both structure and rheological properties of acacia gum dispersions (13). From high-performance size exclusion chromatography-multiangle laser light scattering (HPSEC-MALLS) measurements, it was tentatively suggested that acacia gum molecules displayed a random coil shape. In this study, we combined HPSEC-MALLS, small-angle neutron scattering (SANS) coupled to ab initio calculations, and various microscopic techniques to provide the first model (to our knowledge) for the arabinogalactan from acacia gum.

MATERIALS AND METHODS

Materials

Powdered acacia gum (lot 97J716) from *Acacia senegal* trees was a gift from the CNI company (Rouen, France). Before purification, acacia gum was extensively dialyzed against deionized water and freeze-dried. All chemicals were of analytical grade and were obtained from Merck (Darmstadt, Germany), Sigma (Poole, Dorset, UK), and Aldrich (Deisenhofen, Germany).

Purification of molecular fractions

The main molecular fraction of acacia gum, AG, defined as F1 in the following, was purified as described previously (14). The purified fraction was freeze-dried before further characterization.

High-performance size exclusion chromatography-multiangle laser light scattering

The determination of molecular weight and size distributions of F1 was performed by coupling on-line to an HPSEC, a MALLS detector, a differential refractometer, an ultraviolet (UV) detector, and a differential viscosimeter. F1 dispersions at 0.04 wt % into 50 mM $NaNO_3$ buffer containing 0.02% NaN_3 as preservative were filtered through 0.2-μm Anotop membranes (Anotop, Alltech, France) and injected at 25°C on an HPSEC system constituted of a Shodex (Munich, Germany) OH SB-G precolumn followed by two Shodex OH-pack 804 HQ and 805 HQ columns used in series. The samples were eluted at 0.7 ml min^{-1} with a 50 mM $NaNO_3$ solution. On-line molecular weight and intrinsic viscosity determinations were performed at room temperature using a MALLS detector (mini-Dawn; Wyatt, Santa Barbara, CA; operating at three angles: 41°, 90°, and 138°), a differential refractometer (ERC 7547 A) ($dn/dc = 0.146$ ml g^{-1}), a UV detector ($\lambda =$ 280 nm), and a differential viscosimeter (T-50A; Viscotek, Crowthorne, UK). Weight (M_w) and number (M_n) average molecular weights (g/mol) and radius of gyration (R_g, nm) were calculated using Astra 1.4 software (Wyatt). Intrinsic viscosity [η] was calculated using TriSEC software, version 3.0 (Viscotek).

Scattering experiments and data treatment

SANS experiments on filtrated (0.22-μm filters) F1 ($C = 1\%$ w/v) dissolved in 50 mM NaCl solution in 99.8% D_2O was performed at the Laboratoire Louis Brillouin (Saclay, France) using the PAXY instrument. The spectrum was recorded using two different spectrometer configurations: $\lambda = 10$ Å (incident wavelength), $d = 6.74$ m (distance of the sample to the detector), and $\lambda = 6$ Å, $d = 2.04$ m. The range of wave vectors $q = 4\pi/\lambda \sin(\theta/2)$, θ being the scattering angle, covered was from 4.65×10^{-2} to 3.33×10^{-1} nm^{-1} and from 2.56×10^{-1} to 2.86 nm^{-1}. To attain the second q range, the detector was shifted. The data were normalized for transmission and sample path length and divided by the water spectrum. An absolute intensity scale was obtained using the absolute value of water intensity in units of cross section (cm^{-1}). A subtraction of the appropriate incoherent background, taking hydrogen/deuterium exchange on the polymer into account, was realized (15). It was checked that the incoherent background calculated from the $I(q^4) = f(q^4)$ representation at high q values gave the same value. The scattering intensity at a given wave vector q can be written as

$$I(q) = AP(q)S(q) \text{ or } (N_A d^2/(\Delta\rho^2))I(q)/C = MP(q)S(q).$$

P(q) is the ''form factor'' of the particle and S(q) the ''structure factor'', which accounts for intermolecular interactions. The quantity A is a parameter that includes the particles' concentration C, mass M, and density d, the Avogadro number N_A, and the neutron variation between the particle and the solvent $(\Delta\rho)^2$. Experiments were carried out at different F1 concentrations (1, 2, 5, or 10 wt %) and at 1 wt % F1 concentration in D_2O containing different NaCl concentrations (5, 10, 20, 50, 100, and 500 mM). The form factor P(q) of F1 was obtained from the latter experiments at NaCl concentration where intermolecular interactions were negligible and therefore $S(q) = 1$.

The distance distribution function P(r), representing the distribution of distances between any pair of volume elements within the particle, together with the structural parameters derived from P(r), i.e., the maximum dimension of the particle (D_{max}) and the radii of gyration (R_g), were computed from the form factor by the indirect Fourier transform programs GNOM (16,17) and GIFT (18). The R_g parameter was calculated from the P(r) function following the equation (19)

$$R_g^2 = \frac{\int_0^\infty P(r) r^2 \, dr}{2 \int_0^\infty P(r) dr}. \quad (1)$$

Calculation of low resolution models

Low resolution models of F1 were computed ab initio using the program DAMMIN (20). A sphere of diameter D_{max} is filled by a regular grid of points corresponding to a dense hexagonal packing of small spheres (dummy atoms) of radius $r_0 \ll D_{max}$. The structure of this dummy atom model (DAM) is defined by a configuration vector X assigning an index to each atom corresponding to solvent (0) or solute particle (1). The scattering intensity from the DAM for a given configuration X is computed as

$$I(\mathrm{q}) = 2\pi^2 \sum_{\mathrm{l}=0}^{\infty} \sum_{\mathrm{m}=-\mathrm{l}}^{\mathrm{l}} |A_{\mathrm{lm}}(\mathrm{q})|^2, \quad (2)$$

where the partial amplitudes are given by the equation (20)

$$A_{\mathrm{lm}}(\mathrm{q}) = i^{\mathrm{l}} \sqrt{2/\pi} \sum_{\mathrm{j}} j_{\mathrm{l}}(\mathrm{q} r_{\mathrm{j}}) Y_{\mathrm{lm}}^{+}(\omega_{\mathrm{j}}), \quad (3)$$

where the sum runs over the dummy atoms with $X_j = 1$ (particle atoms), r_j and ω_j are their polar coordinates, and $j_l(x)$ denotes the spherical Bessel function. The number of dummy atoms in the search model $M_{DAM} \approx (D_{max}/r_0)^3 \gg 1$ significantly exceeds the number of Shannon channels. To reduce the effective number of free parameters in the model, the method searches for a configuration X minimizing the function $f(X) = \chi^2 + \alpha P(X)$. Here, χ denotes the discrepancy between the calculated and the experimental curves and is given by

$$\chi = \sqrt{\frac{1}{N-1} \sum_{\mathrm{j}=1}^{\mathrm{N}} \left[\frac{I(\mathrm{q}_{\mathrm{j}}) - I_{\mathrm{exp}}(\mathrm{q}_{\mathrm{j}})}{\sigma(\mathrm{q}_{\mathrm{j}})} \right]^2}, \quad (4)$$

where N is the number of experimental points and $I_{exp}(q_j)$ and $\sigma(q_j)$ are the experimental intensity and its standard deviation, respectively. The looseness penalty term P(X) ensures that the configuration X yields a compact and interconnected structure, and $\alpha > 0$ ensures that the DAM has low resolution with respect to the packing radius r_0. The weight of the penalty is selected to have significant penalty contribution at the end of the minimization. The latter is performed starting from a random approximation using the simulated annealing. Details of the method are described elsewhere (20). The spatial resolution provided by the DAM is defined by the range of the momentum transfer as $\delta r = 2\pi/q_{max}$.

Before the shape analysis, a constant is subtracted from the experimental data to ensure that the intensity decays as q^{-4} following Porod's law (21) for homogeneous particles. The value of this constant is determined automatically by DAMMIN from the outer part of the curve by linear regression in coordinates $q^4 I(q)$ versus q^4. This procedure yields an approximation of the ''shape scattering'' curve (i.e., scattering because of the excluded volume of the particle filled by a constant density).

Furthermore, DAMMIN allows the incorporation of additional information about particle shape, symmetry, and anisometry. This is especially useful for highly anisotropic particles (22). In the case here, the shape and anisometry of particles were set for F1 to ellipsoid and oblate, respectively. Particle symmetry was set to P1 (default parameter). The different parameters, including the dimensions of particles, were chosen based both on the shape of p(r) functions, the values of χ^2 found performing a number of runs while varying shapes and anisometry of particles, and on the use of the PRIMUS program, which contains the BODIES program, which is able to fit experimental scattering curves with three-dimensional geometrical bodies such as ellipsoid, ellipsoid of revolution, cylinder, elliptic cylinder, or hollow cylinder (23).

DAMMIN can perform ab initio calculations using four different modes: fast, slow, jagged and expert. Fast mode is useful for simple particle geometries; however more complex geometries require the use of slow, jagged, or expert modes. After checking the results obtained using the four modes for F1, 12 independent reconstructions were performed using the slow mode. Using the program package DAMAVER, the different reconstructions were averaged, improving the quality of shape reconstruction (24). The program performs the calculation of a normalized spatial discrepancy (NSD) among the different calculated structures, estimating the reliability of the solution. The most probable solution was estimated using the program SUPCOMB (24). This program allows the determination of the NSD parameter d, which is a quantitative estimate of the similarity between two different three-dimensional objects.

To further assess the most probable DAM, we calculated its hydrodynamic parameters using the program HYDROPRO (25), which generates a model from the DAM coordinates, using surface bead sizes that vary between two values specified by the user, to represent the surface of the molecule. This is possible because a model derived from DAMMIN represents a hydrated structure.

Microscopic methods

TEM and cryo-TEM

F1 dispersions at 1 wt % were prepared in deionized water containing 50 mM NaCl. A drop of each dispersion was first placed on a carbon-coated transmission electron microscopy (TEM) copper grid (Quantifoil, Jena, Germany) and allowed to air dry. The sample was then negatively stained with uranyl acetate (Merck). For that, the sample-coated TEM grid was successively placed on a drop of an aqueous solution of uranyl acetate (2% w/w) and on a drop of distilled water. The grid was then air dried before introducing it in the electron microscope. The samples were viewed either using a JEOL JEM-100S TEM or a JEOL JEM-1230 TEM (JEOL, Tokyo, Japan) operating at 80 kV.

All the specimens for cryo-TEM observations were prepared using a cryoplunge cryofixation device (Gatan, Pleasanton, CA) in which drops of the aqueous F1 suspensions were deposited onto glow-discharged holey-type carbon-coated grids (Ted Pella, Redding, CA). Each TEM grid was prepared by blotting a drop containing the specimen to a thin liquid layer of ~50–500 nm in thickness remaining across the holes in the support carbon film. The liquid film was vitrified by rapidly plunging the grid into liquid ethane cooled by liquid nitrogen. The vitrified specimens were mounted in a Gatan 910 specimen holder (Gatan) that was inserted into the microscope using a cryotransfer system (Gatan) and cooled with liquid nitrogen. The TEM images were then obtained from specimens preserved in vitreous ice and suspended across a hole in the supporting carbon substrate. The samples were observed under low dose conditions (<10 e−/A^2) at −178°C, using a JEM 1230 Cryo microscope (JEOL) operated at 80 kV and equipped with a LaB6 filament. All the micrographs were recorded on a Gatan 1.35 K × 1.04 K × 12 bit ES500W Erlangshen charge-coupled device (CCD) camera. Pictures obtained from TEM and cryo-TEM were treated using the ImageJ freeware v1.35c.

Atomic force microscopy

F1 dispersions at 1 wt % were prepared in deionized water containing 50 mM NaCl. An aliquot of 30 μl of this stock solution was diluted in 1 ml

distilled water, and 50 μl of this solution was air dried onto a 10 × 10 mm mica sheet. Before imaging, the samples were rinsed with distilled water and air dried. The atomic force microscopy (AFM) observations were carried out in air. A Dimension 3000 scanning probe microscope equipped with a Nanoscope IIIa controller (Veeco Instruments, Woodbury, NY) was used. The microscope was equipped with TESPD tips (Veeco Instruments), and acquisition was performed in tapping mode at a scan rate of 1 Hz. Pictures were treated directly using the Nanoscope software.

RESULTS AND DISCUSSION

HPSEC-MALLS measurements

Weight average molecular weight (M_w), intrinsic viscosity [η], and radius of gyration R_g of the AG molecular fraction from acacia gum (F1) were determined by HPSEC-MALLS. The relationship between [η] and M_w is shown in Fig. 1. It was first observed from the HPSEC elution profile that most F1 had an M_w around 3×10^5 g/mol, with a few smaller ($M_w \sim 7 \times 10^4$ g/mol) or larger ($M_w \sim 10^6$ g/mol) macromolecules. The polydispersity of the sample was quite low (M_w/M_n: 1.28), which is a necessary condition to properly study the [η] = f(M_w) relationship. As shown in Fig. 1, the log-log plot was linear and it was then possible to fit the data by the Mark-Houwink-Sakurada equation

$$[\eta] = KM_w^{\alpha}, \tag{5}$$

where $\alpha = 0$ for a sphere, 1.8 for a rod, and 0.5–0.8 for flexible chains in ''marginal'' and ''good'' solvents (26). Chain polymers with rigid or asymmetric structures have an α-exponent value >0.6; ionized polyelectrolytes α-exponent values are between 1.0 and 1.7 (27). The parameter K is partly related to the solvent polarity (28), and for flexible chains it typically ranges from 10^{-6} to 10^{-4} mL/g (27). A K value of 5.9×10^{-4} mL/g and an α value of 0.46 were obtained from linear fitting. A value of 0.46 indicated that water was not a good solvent for F1.

This was a somewhat unexpected result since it is generally considered that acacia gum is a rather hydrophilic biopolymer. An α value of 0.47 was reported for total acacia gum (29), the authors indicating that such a value would be indicative of a compact globular structure. Based on this hypothesis, we will show later that it is only partly true, and using M_w and [η], we calculated the hydrodynamic radius (R_h) of F1 following the equation (30)

$$R_h = \left(\frac{3M_w[\eta]}{10\pi N_A}\right)^{\frac{1}{3}}, \tag{6}$$

with N_A the Avogadro number. Results of the calculation are shown in Fig. 2. A linear relationship between R_h and M_w was also found on a log-log plot representation, which indicated that a power law of the form $R_h = KM_w^{\nu}$ also described the data. The exponent ν is a characteristic parameter for a molecular structure. It takes theoretical values of 0.33, 0.60, or 0.50 (in good or moderately good solvent) and 1.0 for homogeneous spheres, random coils, and rigid rods, respectively (31). A ν-exponent value of 0.49, in agreement with a random coil or a star molecule in a moderately good solvent and even a thin disk (31) was found in this study. A value of 0.42 was previously found for total acacia gum (29). From the average F1 M_w of 2.86×10^5 g/mol determined previously (14), a hydrodynamic radius R_h value of 9.3 nm was calculated, a value very close to the experimental R_h of 9.1 nm determined by dynamic light scattering (14). The good agreement between the calculated and experimental R_h values revealed that F1 in solution displayed a sphere-type colloidal behavior. Finally, it was important to notice that R_g

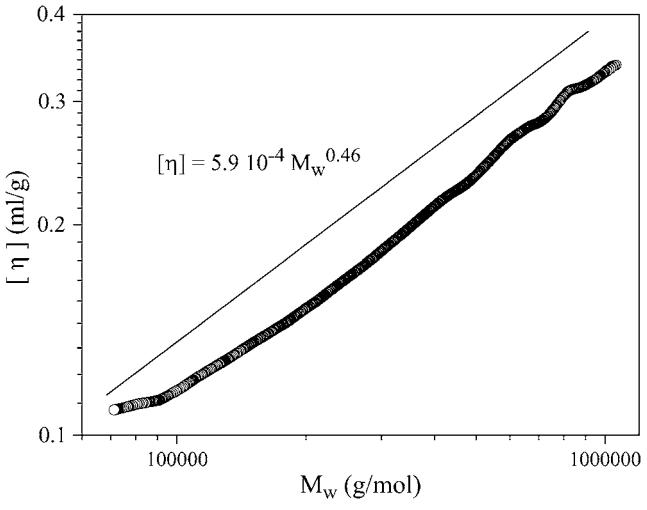

FIGURE 1 Intrintic viscosity [η] (mL/g) as a function of molecular weight (M_w) obtained on the AG-peptide (F1) from acacia gum using HPSEC-MALLS. (*Solid line*) Linear regression fitting of the [η] = f(M_w) experimental data. The fit was translated from experimental data for clarity purposes.

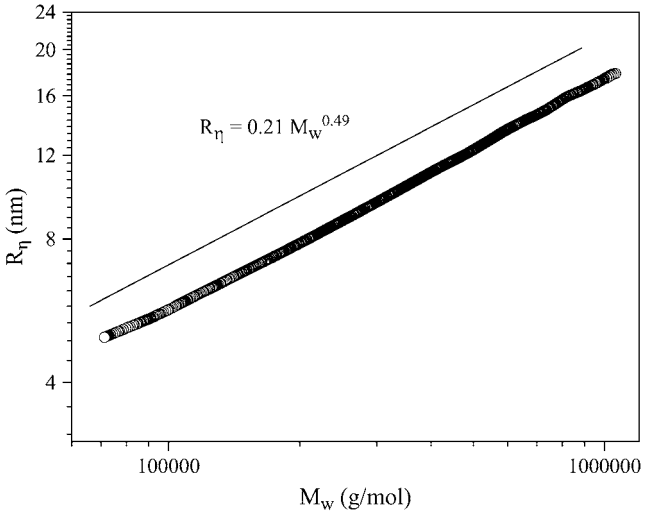

FIGURE 2 Hydrodynamic radius of the AG-peptide F1 as a function of molecular weight (M_w) calculated from [η] results displayed in Fig. 1. (*Solid line*) Linear regression fitting of the R_h = f(M_w) experimental data. The fit was translated from experimental data for clarity purposes.

results given by HPSEC-MALLS software were unreliable, mainly because the majority of macromolecules had an R_g below 10 nm, a value well below the limit of sensitivity of the method.

SANS measurements

A scattering form factor of F1 in D_2O solvent was obtained using SANS. The absence of any correlation peak in the scattering profile demonstrated that 50 mM NaCl was sufficient to suppress intermolecular repulsive interactions (Fig. 3) and indicated too that F1 was a weakly charged polyelectrolyte (14). A similar result was obtained by SANS on total acacia gum (32). The F1 radius of gyration (R_g) was calculated from the Guinier region corresponding to $qR_g < 1$, according to the Guinier approximation $I(q) = I(0)\exp[(-qR_g)^2/3]$, and a value of 6.4 nm was obtained. The shape of F1 may be estimated considering the structure factor $\rho = R_g/R_h$ (31). This ratio is 0.775 for a hard sphere, 1.5 for a monodisperse random coil in good solvent, and >2.0 for a polydisperse random coil or rigid rod ($M_w/M_n = 2.0$). Taking an R_g value of 6.4 nm and an R_h value of 9.1 or 9.3 nm, a ρ value of ~0.7 was found, a value smaller but in the same range as the theoretical value for a hard sphere. The value calculated showed again that F1 adopted in solution a globular structure.

At intermediate scattering wave vectors q, the scattering function I(q) versus q followed a power law of the form $I(q) \sim q^{\alpha}$, with an α value of 2.03. A value of 2 is indicative of the presence of an isolated population of disk-like particles or more generally of a two-dimensional particles morphology (33). From the exponent α, the affinity ν of F1 for the solvent was estimated to be 0.49 ($\alpha = 1/\nu$), a value intermediate between a poor affinity ($\nu = 0.33$) and a very good affinity ($\nu = 0.6$) for the solvent. A value of 0.46 was found from the power law relationship between $[\eta]$ and molecular weight M_w of F1 as determined from HPSEC-MALLS experiments.

At a high q range, where the local structure of scattering objects is probed, scattering intensity followed a power law with an exponent of 2.61. This clearly indicated that the internal structure of F1 was rather dense and ramified.

Since AGPs from acacia gum are commonly described in the literature as highly branched, spheroidal, or random coil-type macromolecules, a fit of the F1 form factor using sphere, random coil (34), and generalized hyperbranched (35) theoretical form factor models was attempted. In the last case, a particle with a fractal dimension of 2.3 and six branches gave the ''best'' fit. However, none of the models was able to satisfactorily fit the F1 form factor (Fig. 4). The possible shape of a macromolecule can be estimated as a first approximation from the shape of the pair distance distribution function P(r), calculated from the form factor P(q) by indirect Fourier transform. The P(r) function of F1 is displayed in Fig. 5. From this function, the maximum distance (D_{max}) found for F1 was of 19.2 nm. R_g calculated from P(r) was of 6.5 nm, a value close to that found from the Guinier approximation ($R_g = 6.4$ nm). Also shown in Fig. 5 are the theoretical P(r) functions for a sphere and a disk (36), both with a diameter of 20 nm. It was deduced from the comparison of the different P(r) functions that F1 more likely had a disk-like morphology.

In addition, the presence of small undulations at distances r above 10 nm could indicate that the flat macromolecule would be inhomogeneous (36). The thickness h of the ''disk'' was roughly estimated from the point where the F(r) function (= P(r)/r) becomes linear (Fig. 6). F1 was found to

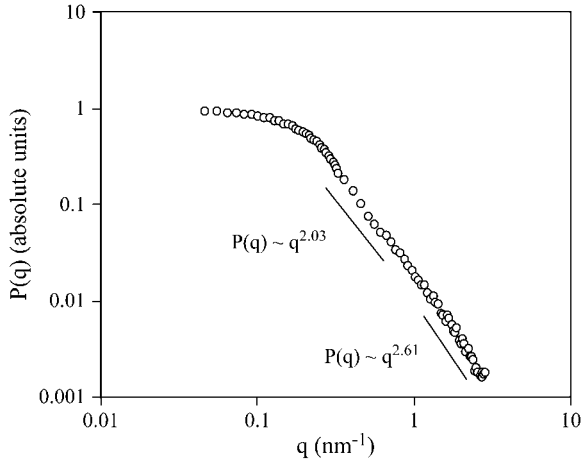

FIGURE 3 AG-peptide F1 scattering form factor (1 w/w%) at 25°C in D_2O containing 50 mM NaCl. The radius of gyration (R_g) was 6.4 nm as calculated from the Guinier region. Please note that the exponent of the power law in the intermediate q range was typical of a population of isolated disks. From the exponent, an affinity for the solvent of 0.49 (1/2.03) was calculated (θ solvent). The exponent at high q range would indicate a rather dense and ramified internal structure.

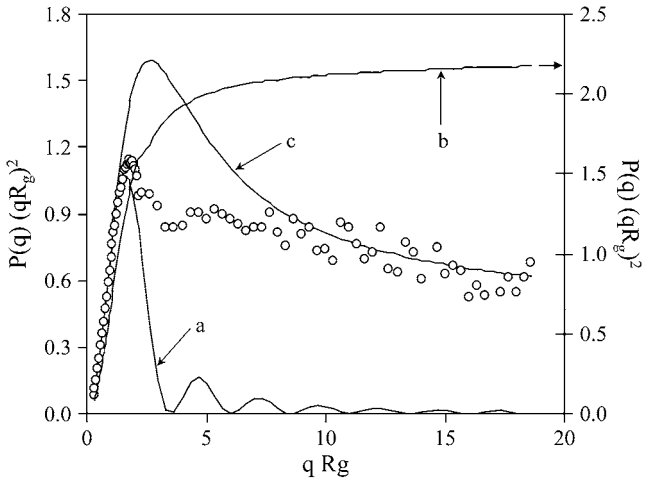

FIGURE 4 Kratky-type plot of the AG-peptide F1 scattering form factor. Theoretical form factors of a sphere (*a*), a Gaussian coil (*b*), and a general hyperbranched polymer with a fractal dimension of 2.3 and 6 branches (*c*) were plotted for comparison.

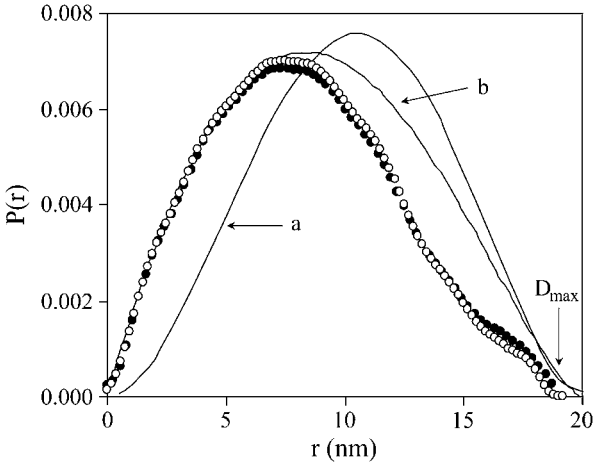

FIGURE 5 Pair distance distribution function P(r) calculated by indirect Fourier transform of the scattering curve of the AG-peptide F1 using GIFT (○) and GNOM (●) software. Maximum dimension of F1 (D_{max}) was 19.2 nm and R_g 6.5 nm. Solid lines are the theoretical P(r) of an infinitely thin circular disk of 20 nm diameter (Porod model) (*a*) and of a sphere of 20 nm diameter (*b*).

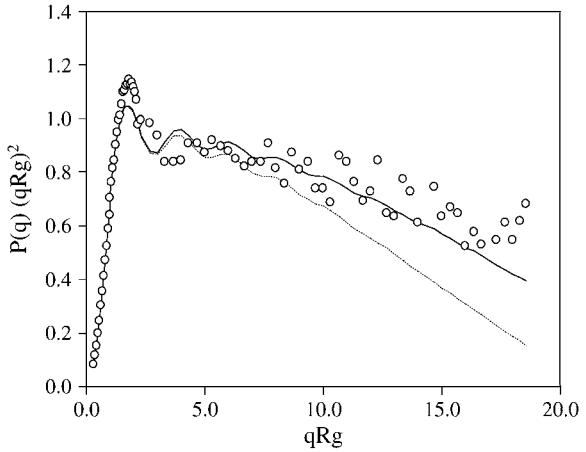

FIGURE 7 Kratky-type plot of the experimental form factor of the AG-peptide F1 (1 w/w%) at 25°C in D_2O containing 50 mM NaCl (○) and of theoretical form factors of an infinitely thin circular disk with 9.6 nm radius and 1.4 nm thickness (*solid curve*) or 9.6 nm radius and 1.9 nm thickness (*dotted curve*).

have a thickness of ~1.9 nm. Using a radius of 9.6 nm and a thickness of 1.9 nm, the F1 form factor was fitted using the theoretical form factor of a thin disk (Fig. 7) (34). The fit was not entirely satisfactory, particularly in the high q range; however, the overall characteristic of the form factor was approached. The best fit was thus obtained using an F1 thickness of 1.4 nm. The thickness h of a flat disk-like macromolecule can be computed from $h = (4M_w)/(\pi D^2 N_A \rho)$, where D is the macromolecule diameter and ρ its density (37). Taking an M_w of 2.86×10^5 g/mol, a diameter of 20 nm, and a density of 1.007 (determined experimentally using a pycnometer), a thickness of 1.5 nm was found, a value very close to the 1.4 nm value used for the fit in Fig. 7. The very low density measured for F1 can be compared to the 1.003 value measured on total acacia gum (38). Moreover, exactly the same value was measured for total acacia gum in our laboratory from which the major molecular fraction F1 was extracted.

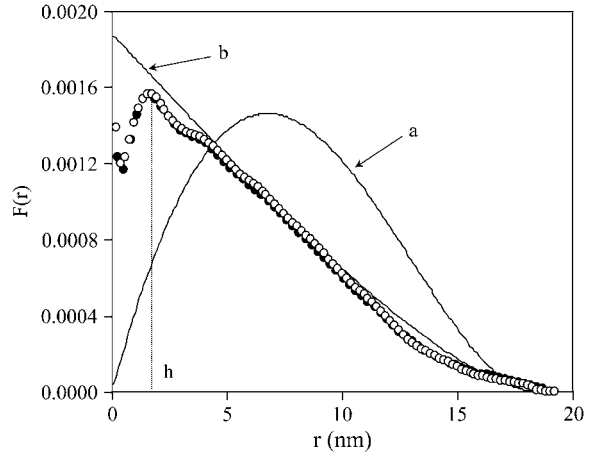

FIGURE 6 F(r) functions calculated from P(r) functions of the AG-peptide F1 obtained using GIFT (○) and GNOM (●) software. The thickness h was estimated from the transition point (*dotted line*) where the curves became mainly linear ($h \sim 1.9$ nm). Solid lines were theoretical F(r) functions of an infinitely thin circular disk of 20 nm diameter (Porod model) (*a*) and of a sphere of 19.2 nm diameter (*b*).

Low resolution models calculation and microscopy

Low resolution DAMs of the AG-peptide F1 from acacia gum were computed using an ab initio approach. To compute these models, the shape and anisometry of F1 were initially set to ellipsoid and oblate, respectively. A prolate anisometry led to a large discrepancy between the calculated and experimental form factors P(q). The symmetry of the particle was left as P1 (default value). Semiaxes a, b, and c of the ellipsoid were set to 9.6, 9.6, and 1.0 nm, respectively.

Whereas DAMs were calculated using the slow calculation mode (12 runs) of DAMMIN software, very similar models could be obtained using the jagged or expert modes. Different views of the most probable DAM for F1 are depicted in Fig. 8. It appeared that F1 was an oblate ellipsoid with an open and highly branched internal structure, the central part forming a kind of intricate network. The form factor calculated from the most probable DAM perfectly matched the experimental form factor (Fig. 9). The discrepancy between the calculated and the experimental curves, defined by the χ parameter, was ~0.64 for the 12 runs, a value corresponding to a reasonable solution. It is worth noting that such an intriguing model was totally unexpected based on the data in the literature.

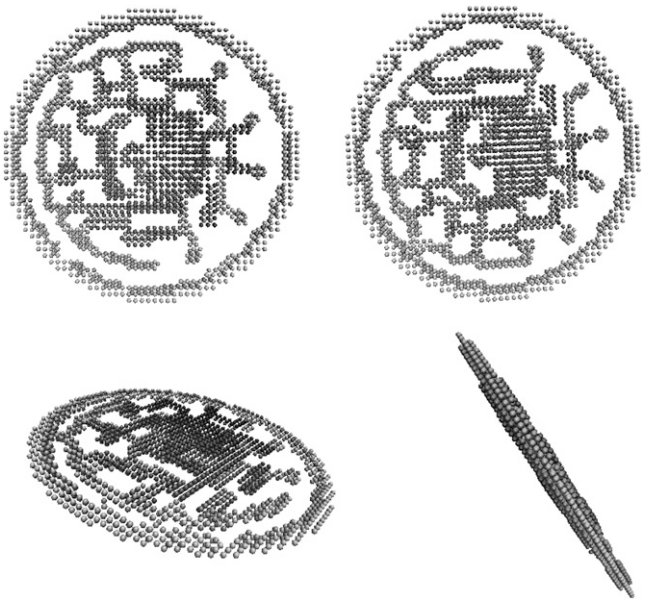

FIGURE 8 Different views of the most probable DAM of F1 obtained using the DAM method as implemented in the program DAMMIN. Calculations were performed imposing ellipsoid shape and oblate anisometry in the program. Semiaxes of the ellipsoid were set to 9.6, 9.6, and 1.0 nm.

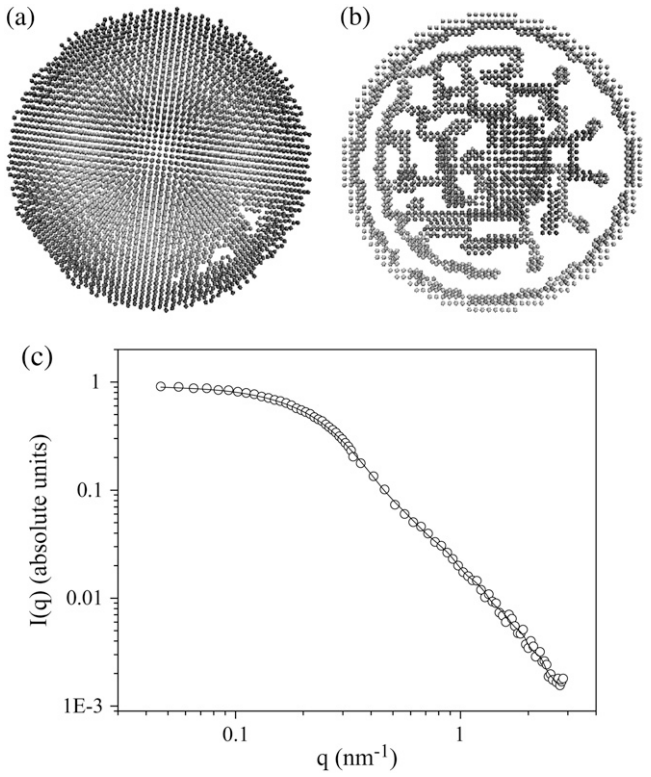

FIGURE 9 Low resolution averaged (*a*) and most probable (*b*) DAM of the AG-peptide F1 from acacia gum (slow calculation mode). The 12 models obtained were analyzed using the package DAMAVER (see Materials and Methods). (*c*) Experimental F1 form factor (1 w/w%) at 25°C in D_2O containing 50 mM NaCl (○) and scattering function from the reconstructed most probable DAM (*solid curve*).

As the most probable DAM only represented a low resolution model that did not necessarily reflect the reality, microscopic experiments using TEM, cryo-TEM, and AFM were performed to check the reliability of the F1 model proposed. TEM, cryo-TEM, and AFM confirmed that F1 had an oblate ellipsoidal shape with a diameter of ~20 nm (Fig. 10). AFM pictures further revealed that the thickness of F1 was below 2 nm (Fig. 10 *c*). TEM micrographs emphasized a difference of contrast between the exterior and interior of ellipsoids, the interior being branched as compared to the exterior (Fig. 10 *a*, *a1*, and *a2*). More details were seen by cryo-TEM after image analysis (Fig. 10 *b*). F1 appeared to be constituted by a kind of ring from which a network-like highly branched structure was linked. A number of branching points could be observed that contrasted somewhat with the more probable DAM where mainly a large branching point could be observed.

After contrast variation and fast Fourier transform (FFT) filtering of the image shown in Fig. 10 *b*, the fractal dimension of the picture using ImageJ freeware was determined and a value of 2.7 was found. This value was in total agreement with the power law exponent value of 2.6 found in the high q range of the F1 form factor (see Fig. 3). If picture *b2* of Fig. 10 was better observed, that is, enlarged in Fig. 11 for the sake of clarity, it appeared that the inner highly branched structure of F1 could be composed of small aggregated subunits with dimensions on the order of ~1.5–2 nm, a value of the same order of the thickness of the outer ring. In addition, it would seem—but this assumption would need to be considered with special care—that these subunits are located in a more or less periodic way. A close look at the most probable DAM of F1 (Fig. 8) also revealed that structural components were regularly spaced, a feature that also appeared in Fig. 10 *b3*.

Only one study using TEM highlighted an ellipsoidal structure for an AGP with dimensions of 15 nm × 25 nm for the major axis (39). It was observed in this study that AGP macromolecules also displayed a higher contrast in the outer part of ellipsoids compared to the inner part, revealing a structural inhomogeneity. The discovery of an ellipsoidal structure was interpreted as an indication of the reliability of the wattle blossom model for AGP. In a more recent study, spheroidal micelle-like aggregates with diameters of ~20 nm were seen by cryo-TEM in total acacia gum (32). However the authors also attributed these structures to the larger component of the gum, i.e., AGP (32). On the other hand, a recent AFM study showed that molecules of total acacia gum had elongated wormlike shapes with maximum dimensions above ~75–100 nm (40). The authors attributed these structures to the main molecular fraction of acacia gum, i.e., the F1 fraction. As pictures were obtained from total acacia gum solution containing Tween 20, a nonionic surfactant, it cannot be excluded that the oblate ellipsoids detected in this

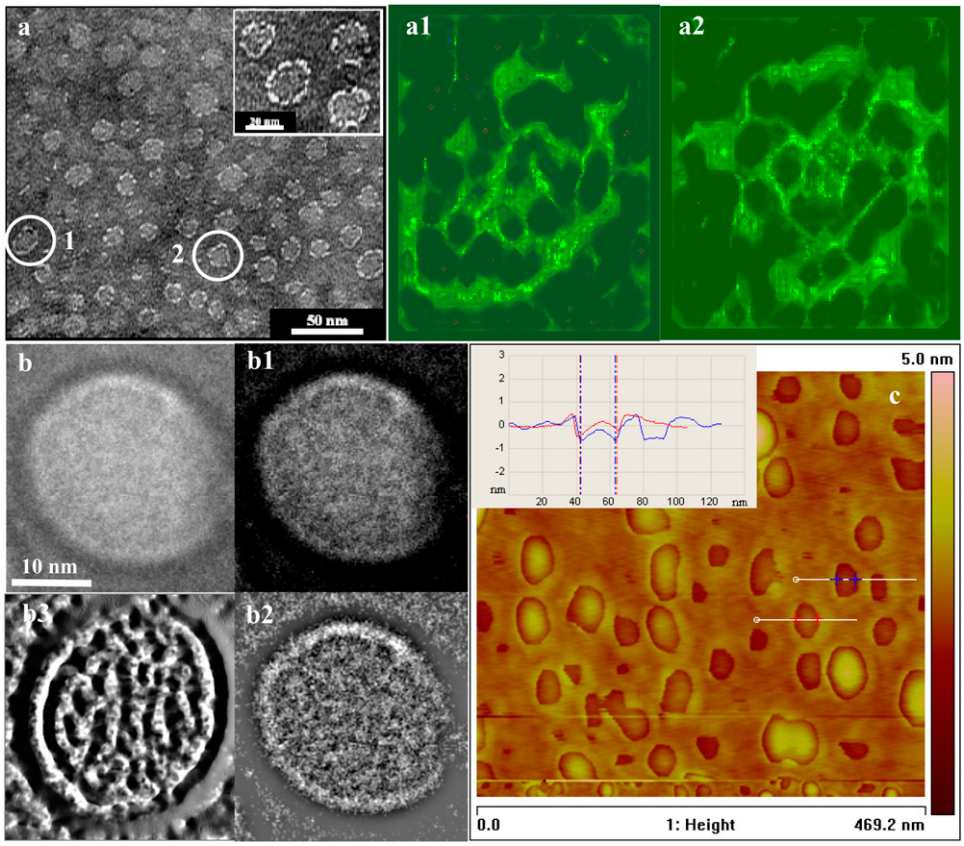

FIGURE 10 (*a*) TEM micrograph of the AG-peptide F1 from acacia gum. (*Inset*) Magnification of part of micrograph 10 *a*, *a1*, *a2*. F1 macromolecules isolated from the TEM micrograph (located in *circles 1* and *2*) but transformed into false colors using the ImageJ freeware v1.35c and treated using the Surface Plot 3D plugin. (*b*) Cryo-TEM micrograph of the AG-peptide F1 macromolecule from acacia gum. (*b1*) Same as *b* after applying contrast variation. (*b2*) Same as *b1* after FFT filtering. (*b3*) Same as *b1* after treatment using the ImageJ freeware v1.35c and the Surface Plot 3D plugin. (*c*) AFM micrograph of the AG-peptide F1 macromolecule from acacia gum obtained after air drying in tapping mode at a scan rate of 1 Hz. (*Inset*) Dimensions of the two F1 macromolecules indicated in *c*.

study could be aggregated structures of individual branched chains, as indirectly suggested by Dror et al. (32). However, the large dimensions found by Ikeda et al. (40) would rather suggest that macromolecules pictured more probably would stem from the large AGP (F2) or GP (F3) fractions of acacia gum (14).

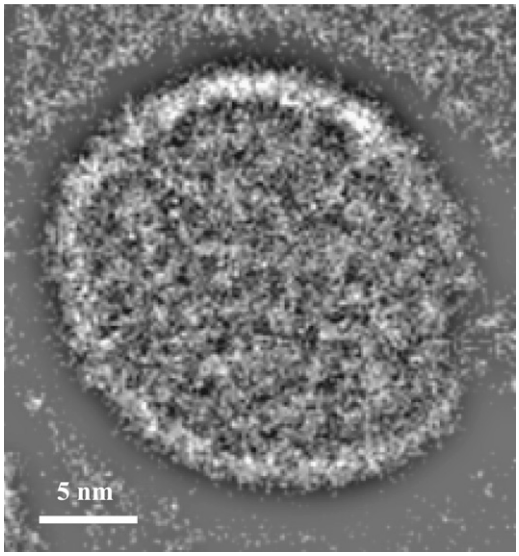

FIGURE 11 Enlargement (×3) of the picture *b2* of Fig. 10.

From the previous results showing that F1 was an oblate ellipsoid with major and minor axes of, respectively, 19.2 and ~1.5 nm, a number of structural and hydrodynamic parameters can be calculated or computed. The theoretical R_g and R_h of an oblate ellipsoid with semiaxes 9.6 and 0.75 nm were 6.1 and 6.4 nm, respectively (41). The resulting structure factor ρ is 0.95, a value higher than the experimental value found ($\rho = 0.70$). This discrepancy can be explained by the fact that the calculated R_h was smaller than the experimental one (9.1 nm), emphasizing both the hydration features and flexibility of F1 in solution. On the other hand, the calculated R_g was in good agreement with R_g (6.5 nm) determined from the pair distance distribution function P(*r*).

Hydrodynamic parameters can also be calculated using the HYDROPRO software based on the most probable DAM of F1 and including in the input file some parameters such as temperature (293.15 K), solvent viscosity (1.003×10^{-3} Pa/s), and both partial specific volume of solvent (0.998 mL/g) and the F1 macromolecule (0.993 mL/g). The results obtained are depicted in Table 1. Maximum dimension of F1 and R_g were in good agreement with the values determined experimentally (Table 1, values in brackets). Significant discrepancies were obtained for D_T, the translational diffusion coefficient, and R_h and especially for $[\eta]$ and the hydrated volume V_H, which was calculated from the equation $V_H = (M_w/N_A)\bar{\nu}_H$ (30), where $\bar{\nu}_H$ is the specific volume of F1 (1.345 mL/g), calculated using the partial specific

TABLE 1 Hydrodynamic parameters calculated from the DAM of the AG-peptide F1 from acacia gum using the HYDROPRO software

	Calculated values
Translational diffusion coefficient D_T (10^7 cm^2/s)	3.05 (2.39)
R_h (nm)	7.0 (9.1)
R_g (nm)	7.2 (6.5)
Hydrated volume V_H (10^{19} cm^3)	1.8 (6.4)
Rotational diffusion coefficient (10^{-5} s^{-1})	2.85
Relaxation (correlation) time (10^7 s)	5.2
$[\eta]$ (mL/g)	7.64 (16.2)
Sedimentation coefficient (S)	0.24 S
D_{max} (nm)	19.7

Calculations were performed using the following parameters: radius of atomic elements 0.3 nm, minimum radius of beads in the shell 0.3 nm, maximum radius of beads in the shell 0.52 nm, temperature 298.15 K, viscosity D_2O 0.011 poises, density of D_2O 1.1044 mL/g, molecular weight of F1 286,000 g/mol, and partial specific volume of F1 0.993 mL/g (density 1.007 g/mL). Values between parentheses corresponded to parameters experimentally measured or calculated.

volumes of solvent and F1 and the F1 hydration parameter (bound water: 0.35 g/g) (42). These discrepancies can be attributed both to the calculation method and specific structure of F1. Regarding the calculation, hydrodynamic parameters are computed on a model that is first filled with beads based on the assumption that macromolecules are rigid (25), uncharged, and impenetrable (43). However, F1 was mostly flexible and displayed an open ''porous'' highly branched structure, able to bind not only 0.5 g/g of tightly bound water but also a total amount of ~3 g/g water (44). These features are likely to explain the larger calculated hydrated volume of F1 and its lower translational diffusion coefficient. Table 2 summarized the main structural and hydrodynamic parameters determined in this study for the AG-peptide main molecular fraction F1 from acacia gum.

TABLE 2 Summary of F1 structural and hydrodynamic parameters experimentally determined by HPSEC-MALLS, SANS, and the pycnometric method, or calculated

Structural and hydrodynamic parameters	Values
M_w (g/mol)	2.86×10^5
M_w/M_n	1.28
Semiaxes $a/b/c$ (nm)	9.6/9.6/0.75
D_{max} (nm)	19.2
R_g (nm)	6.5; 6.1*
R_h (nm)	9.1†; 9.3‡; 6.4§
Translational diffusion coefficient D_T (10^7 cm^2/s)	2.39
$[\eta]$ (ml/g)	16.2
Density	1.007
Partial specific volume (ml/g)	0.993
Specific volume (ml/g)	1.345
Hydration parameter δ (g/g)	0.35¶
Hydrated volume V_H (ml)	6.4×10^{-19}
Flory-Fox parameter ϕ	11.5×10^{23}‖
α-exponent	0.46**
ν-exponent	0.49††
Solvent affinity	0.49‡‡
D_{frac}	2.03§§
Scattering length density (cm^{-2})	3.2×10^{10}¶¶

*Theoretical R_g of a disk with semiaxes a and b following $R_g^2 = 0.2\,(2a^2+b^2)$.
†Determined by dynamic light scattering at three angles (30°, 90°, and 150°).
‡Calculated from the equation $[\eta] = 6.308 \times 10^{24}\, R_h^3/M_w$ (30).
§Theoretical R_h of a disk with semiaxes a and b following $R_h = [b(a^2/b^2 - 1)^{0.5}]/a\ \tan[(a^2/b^2 - 1)^{0.5}]$.
¶Taken from Phillips et al. (42).
‖From the Flory-Fox equation $\phi = [\eta]\, M_w/6^{3/2}\, (R_g)^3$.
**From the Mark-Houwink-Sakuruda equation $[\eta] = KM_w^{\alpha}$.
††From the equation $R_h = KM_w^{\nu}$.
‡‡$1/d_f$.
§§Determined in the intermediate q range from the power law $I(q) \sim q_f^{-d}$.
¶¶Calculated from contrast variation measurements (matching F1 scattering intensity for D_2O 49.8% in NaCl 23 mM).

CONCLUSION

The disk-like model of the AG-peptide from acacia gum, derived from SANS and microscopy, is the first model, to our knowledge, involving an AG-peptide in solution. However, our model would appear difficult to conciliate with the proposed wattle blossom model. In the latter case, outer polysaccharides domains were linked to a central short polypeptide backbone, forming a spheroidal random coil. In our model, considering further that 98% of residues were sugars (14), the inner branched structure and the ring should be necessarily mainly composed by sugars. Polysaccharide domains would thus be in the interior of the particle, resulting in a highly organized open disk-like structure.

It is difficult at this stage to draw relationships between the revealed F1 structure and its physicochemical and biological properties. However, some preliminary assumptions can be addressed. Previous literature argued that acacia gum would be synthesized in the cambial zone where there is no gradient for its transport (45). However, the questionable argument given by the authors was that the gum macromolecules did not need gradient to be transported from the site of biosynthesis to the point of exudation. A more realistic argument was given in an anatomical study of wood and bark of *A. senegal* trees that clearly demonstrated that the site of biosynthesis of the gum took place in the inner phloem (46). This tissue is known to be in charge of the transport of solutes and macromolecules in plants. This study revealed that the structural dimensions found would be in agreement with a phloem-mediated long-distance transport.

The open structure and the high flexibility of F1 (the persistence length is at best on the order of 3 nm; results not shown) could explain the anomalous low viscosity of acacia gum solutions in comparison to most known polysaccharides (47). The network-like morphology of the disk with the presence of charged sugar residues could play a role in the known self-assembly properties of AGP-like macromolecules and their ability to interact with proteins (13,48). Molecular modeling tools on models built to gain deeper insights into the F1 structure will be planned in the near future, as well as the

determination of the conformation in solution of the other acacia gum molecular fractions, i.e., the AGP fraction and the various GPs found in the third molecular fraction of acacia gum. The main idea will be in particular to know if the presence of higher protein content in these two molecular fractions may confer differences in the structural characteristics of macromolecules.

REFERENCES

1. Majewska-Sawka, A., and E. A. Nothnagel. 2000. The multiple roles of arabinogalactan proteins in plant development. *Plant Physiol.* 122:3–9.
2. Gaspar, Y. M., K. L. Johnson, J. A. McKenna, A. Bacic, and C. J. Schultz. 2001. The complex structure of arabinogalactan-proteins and the journey towards understanding function. *Plant Mol. Biol.* 47: 161–176.
3. Showalter, A. M. 2001. Arabinogalactan-proteins: structure, expression and function. *Cell. Mol. Life Sci.* 58:1399–1417.
4. Rumyantseva, N. I. 2005. Arabinogalactan proteins: involvement in plant growth and morphogenesis. *Biochemistry (Mosc.).* 70:1073–1085.
5. Verbeken, D., S. Dierckx, and K. Dewettinck. 2003. Exudate gums: occurrence, production, and applications. *Appl. Microbiol. Biotechnol.* 63:10–21.
6. Anderson, D. M. W., and J. F. Stoddart. 1966. Studies on uronic acid materials—Part XV: the use of molecular sieve chromatography in studies on *Acacia senegal* gum (gum arabic). *Carbohydr. Res.* 2: 104–114.
7. Churms, S. C., E. H. Merrifield, and A. M. Stephen. 1983. Some new aspects of the molecular structure of *Acacia senegal* gum (gum arabic). *Carbohydr. Res.* 123:267–279.
8. Anderson, D. M. W., M. M. E. Bridgeman, J. G. K. Farquhar, and C. G. A. McNab. 1983. The chemical characterization of the test article used in toxicological studies of gum arabic (*Acacia senegal* (L.) Willd). *Intern. Tree Crops J.* 2:245–254.
9. Randall, R. C., G. O. Phillips, and P. A. Williams. 1989. Fractionation and characterisation of gum from *Acacia senegal*. *Food Hydrocoll.* 3:65–75.
10. Fincher, G. B., B. A. Stone, and A. E. Clarke. 1983. Arabinogalactan-proteins: structure, biosynthesis, and function. *Ann. Rev. Plant Physiol.* 34:47–70.
11. Qi, W., C. Fong, and D. T. A. Lamport. 1991. Gum arabic is a twisty hairy rope. *Plant Physiol.* 96:848–855.
12. Carpita, N. 1982. Limiting diameters of pores and the surface structure of plant cell walls. *Science.* 218:813–814.
13. Sanchez, C., D. Renard, P. Robert, C. Schmitt, and J. Lefebvre. 2002. Structure and rheological properties of acacia gum dispersions. *Food Hydrocoll.* 16:257–267.
14. Renard, D., L. Lavenant-Gourgeon, M.-C. Ralet, and C. Sanchez. 2006. *Acacia senegal* gum: continuum of molecular species differing by their protein to sugar ratio, molecular weight, and charges. *Biomacromolecules.* 7:2637–2649.
15. Brulet, A., D. Lairez, A. Lapp, and J. P. Cotton. 2007. Improvement of data treatment in small-angle neutron scattering. *J. Appl. Crystallogr.* 40:165–177.
16. Svergun, D. I., A. V. Semenyuk, and L. A. Feigin. 1988. Small-angle-scattering-data treatment by the regularization method. *Acta Crystallogr.* A44:244–250.
17. Svergun, D. I. 1992. Determination of the regularization parameter in indirect-transform methods using perceptual criteria. *Appl. Cryst.* 25: 495–503.
18. Glatter, O. 1977. A new method for the evaluation of small-angle scattering data. *J. Appl. Crystallogr.* 10:415–421.
19. Glatter, O. 1982. Data treatment. *In* Small Angle X-Ray Scattering. O. Glatter and O. Kratky, editors. Academic Press, London. 119–165.
20. Svergun, D. I. 1999. Restoring low resolution structure of biological macromolecules from solution scattering using simulated annealing. *Biophys. J.* 76:2879–2886.
21. Porod, G. 1982. General theory. *In* Small Angle X-Ray Scattering. O. Glatter and O. Kratky, editors. Academic Press, London. 18–51.
22. Volkov, V. V., and D. I. Svergun. 2003. Uniqueness of ab initio shape determination in small-angle scattering. *J. Appl. Cryst.* 36:860–864.
23. Konarev, P. V., V. V. Volkov, A. V. Sokolova, M. H. J. Koch, and D. I. Svergun. 2003. PRIMUS: a Windows PC-based system for small-angle scattering data analysis. *J. Appl. Crystallogr.* 36:1277–1282.
24. Kozin, M. B., and D. I. Svergun. 2001. Automated matching of high- and low-resolution structural models. *J. Appl. Crystallogr.* 34: 33–41.
25. Garcia de la Torre, J., M. L. Huertas, and B. Carrasco. 2000. Calculation of hydrodynamic properties of globular proteins from their atomic-level structure. *Biophys. J.* 78:719–730.
26. Ross-Murphy, S. B. 1994. Rheological methods. *In* Physical Techniques for the Study of Food Biopolymers. S. B. Ross-Murphy, editor. Blackie Academic & Professional, London. 343–392.
27. Kawahigashi, M., H. Sumida, and K. Yamamoto. 2005. Size and shape of soil humic acids estimated by viscosity and molecular weight. *J. Coll. Interf. Sci.* 284:463–469.
28. Shen, Q., D. Mu, L.-W. Yu, and L. Chen. 2004. A simplified approach for evaluation of the polarity parameters for polymer using the *K* coefficient of the Mark–Houwink-Sakurada equation. *J. Coll. Interf. Sci.* 275:30–34.
29. Idris, O. H. M., P. A. Williams, and G. O. Phillips. 1998. Characterisation of gum from *Acacia senegal* trees of different age and location using multidetection gel permeation chromatography. *Food Hydrocoll.* 12:379–388.
30. Tanford, C. 1961. Transport processes—viscosity. *In* Physical Chemistry of Macromolecules. C. Tanford, editor. John Wiley & Sons, New York. 391.
31. Burchard, W. 1994. Light scattering techniques. *In* Physical Techniques for the Study of Food Biopolymers. S. B. Ross-Murphy, editor. Blackie Academic & Professional, London. 151–213.
32. Dror, Y., Y. Cohen, and R. Yerushalmi-Rozen. 2006. Structure of gum arabic in aqueous solution. *J. Polym. Sci. Part B—Polym. Phys.* 44: 3265–3271.
33. Svergun, D. I., and M. H. J. Koch. 2003. Small-angle scattering studies of biological macromolecules in solution. *Rep. Prog. Phys.* 66:1735–1782.
34. Pedersen, J. S. 1997. Analysis of small-angle scattering data from colloids and polymer solutions: modeling and least-squares fitting. *Adv. Coll. Interf. Sci.* 70:171–210.
35. Burchard, W. 2004. Angular dependence of scattered light from hyperbranched structures in a good solvent. A fractal approach. *Macromolecules.* 37:3841–3849.
36. Glatter, O. 1982. Interpretation. *In* Small Angle X-Ray Scattering. O. Glatter and O. Kratky, editors. Academic Press, London, 167–196.
37. Goring, D. A. I., R. Vuong, G. Cancet, and H. Chanzy. 1979. The flatness of lignosulfonate macromolecules as demonstrated by electron microscopy. *J. Appl. Polym. Sci.* 24:931–936.
38. Holleman, V. L. W. J., and H. G. Bungenberg de Jong. 1916. Elektroviskoser effekt und umladung von natriumarabinatsolen durch neutralsalze mit 1-, 2- und 3 wertigen kationen. *Koll.-Beihefte Band* 46: 113–133.
39. Baldwin, T. C., M. C. McCann, and K. Roberts. 1993. A nove1 hydroxyproline-deficient arabinogalactan protein secreted by suspension-cultured cells of daucus carota. *Plant Physiol.* 103: 115–123.
40. Ikeda, S., T. Funami, and G. Zhang. 2005. Visualizing surface active hydrocolloids by atomic force microscopy. *Carbohydrate Polym.* 62:192–196.

41. Slayter, H., J. Loscalzo, P. Bockenstedt, and R. I. Handin. 1985. Native conformation of human von Willebrand protein. *J. Biol. Chem.* 260: 8559–8563.

42. Phillips, G. O., S. Takigami, and M. Takigami. 1996. Hydration characteristics of the gum exudate from *Acacia senegal*. *Food Hydrocoll.* 10:11–19.

43. Winzor, D. J., L. E. Carrington, and S. E. Harding. 2001. Analysis of thermodynamic non-ideality in terms of protein solvation. *Biophys. Chem.* 93:231–240.

44. Takigami, S., M. Takigami, and G. O. Phillips. 1995. Effect of preparation method on the hydration characteristics of hylan and comparison with another highly cross-linked polysaccharide, gum arabic. *Carbohydr. Polym.* 26:11–18.

45. Joseleau, J.-P., and G. Ullmann. 1990. Biochemical evidence for the site of formation of gum arabic in *Acacia senegal*. *Phytochemistry.* 29:3401–3405.

46. Ghosh, S. S., and S. K. Purkayastha. 1962. Anatomical studies of wood and bark of *Acacia senegal* Willd. trees with special reference to gum exudation. *Indian Forester.* 88:92–100.

47. Redgwell, R. J., C. Schmitt, M. Beaulieu, and D. Curti. 2005. Hydrocolloids from coffee: physicochemical and functional properties of an arabinogalactan-protein fraction from green beans. *Food Hydrocoll.* 19:1005–1015.

48. Schmitt, C., C. Sanchez, F. Thomas, and J. Hardy. 1999. Complex coacervation between β-lactoglobulin and acacia gum in aqueous medium. *Food Hydrocoll.* 13:483–496.